KRÄMER, V. (1975). *Acta Cryst.* B31, 234–237.
MERCIER, P. R., DOUGLADE, J. & THEOBALD, F. (1975). *Acta Cryst.* B31, 2081–2085.
MOORE, P. B. & ARAKI, T. (1976). *Neues Jb. Miner. Mh.* In the press.
POORE, M. C. & RUSSELL, D. R. (1971). *Chem. Commun.* pp. 18–20.
ROGERS, D. & SKAPSKI, A. C. (1964). *Proc. Chem. Soc.* pp. 400–401.
SILLÉN, L. G. & MELANDER, L. (1941). *Z. Kristallogr.* **103**, 420–430.
SKAPSKI, A. C. & ROGERS, D. (1965). *Chem. Commun.* pp. 611–613.
SVENSSON, C. (1974). *Acta Cryst.* B30, 458–461.
SVENSSON, C. (1975). *Acta Cryst.* B31, 2016–2018.
SÄRNSTRAND, C. (1974). *Acta Chem. Scand.* A28, 275–283.
SÄRNSTRAND, C. (1976*a*). To be published.
SÄRNSTRAND, C. (1976*b*). To be published.
ÅSTRÖM, A. & ANDERSSON, S. (1971). *Acta Chem. Scand.* **25**, 1519–1520.
ÅSTRÖM, A. & ANDERSSON, S. (1973). *J. Solid State Chem.* **6**, 191–194.

Acta Cryst. (1976). B32, 1777

Charge Density Studies Below Liquid Nitrogen Temperature. II. Neutron Analysis of *p*-Nitropyridine *N*-Oxide at 30K and Comparison with X-ray Results

BY P. COPPENS*

Institut Laue–Langevin et Laboratoires des Rayons-X, CNRS, Avenue des Martyrs, 38042 *Grenoble, France*

AND M. S. LEHMANN

Institut Laue–Langevin, B.P. n° 156, 38042 *Grenoble, France*

(*Received* 6 *November* 1975; *accepted* 15 *December* 1975)

The earlier 30K X-ray analysis of *p*-nitropyridine *N*-oxide has been complemented with a low-temperature neutron diffraction study. Analysis of the X–N deformation densities at different data cut-off values indicates an effect of series termination on lone-pair and also bond densities, which can be accounted for by a quantitative analysis within a single Gaussian approximation to the density peaks. The nitroxo group lone-pair densities are situated at right angles to the NO bond axis. Comparison with other X–N densities leads to differences in hybridization between NO and CO oxygen atoms, the former having a $p\,\sigma$-bonding orbital and non-hybridized *s* and *p* lone-pair orbitals. No bonding electrons are observed in the terminal NO bonds.

Introduction

The present study is a continuation of the charge density analysis of *p*-nitropyridine *N*-oxide described recently (Wang, Blessing, Ross & Coppens, 1976). To complement the earlier work, neutron data have been collected at the high-flux beam reactor of the Institut Laue–Langevin. Of special interest are the nature of the bonding in the nitroxo and nitro substituents, the resolution achievable and the magnitude of series termination effects in charge density studies at very low temperatures.

Data collection and refinement

Neutron data were collected on the four-circle diffractometer D10 located at a thermal neutron guide of the Institut Laue–Langevin high-flux beam reactor. Low temperature was achieved with a liquid He cryostat (Claudet, Tippe & Yelon, 1976) which has a temperature stability of better than 0·5°. Cell dimensions were taken from the earlier X-ray analysis and are listed with other crystallographic information in Table 1.

Table 1. *Crystal data*

Numbers in parentheses here and under similar conditions throughout the paper are estimated standard deviations in units of the last digit.

Space group *Pnma*; $Z=4$; $\mu=1{\cdot}52\ (2)\ \text{cm}^{-1}$; $\varrho_c=1{\cdot}637\ \text{g cm}^{-3}$
$a=12{\cdot}498\ (6)$, $b=5{\cdot}814\ (2)$, $c=7{\cdot}824\ (2)$ Å

$(\sin\theta/\lambda)_{\max}$: 0·55 Å^{-1}
Measurement temperature: 30K
Total number of reflexions: 1456
Number of unique reflexions: 451

A crystal 13·5 mm^3 showing the forms {111}, {100} and the face (001) was used for data collection and oriented with **c** close to, but not coinciding with, the φ axis of the diffractometer. The construction of the cryostat prevents centring after cooling, but crystal orientation and measurements at both positive and

* Permanent address: Chemistry Department, State University of New York at Buffalo, Buffalo, N.Y. 14214, U.S.A.

negative 2θ values indicated that the crystal had not moved more than a maximum 0·2 mm, which is acceptable because of the good homogeneity of the neutron beam.

Reflexion against the (111) plane of a Cu crystal was used to obtain a monochromatic beam with $\lambda = 1{\cdot}445$ Å, and a flux of 10^6 n cm^{-2}s^{-1}. As the neutron guide tube provides a highly collimated beam with angular divergence of about 10′ it was possible to use an ω scan for data collection. This eliminates a background correction for Al powder lines from the cryostat window. Nevertheless for a few reflexions some indications of preferred orientation in the Al window were observed. 68 out of 1456 reflexions were eliminated on careful examination of their profiles. Profiles were reduced to F^2 values with the minimal $\sigma(I)/I$ criterion (Lehmann & Larsen, 1974) where I is the integrated intensity and $\sigma(I)$ its standard deviation. Absorption corrections were applied by the Gaussian numerical integration method with an experimental absorption coefficient determined by transmission measurements of four crystals. The transmission factor of the sample crystal varied between 0·70 and 0·79. Two octants of reflexions (k both positive and negative) were measured with $(\sin\theta/\lambda)_{max} = 0{\cdot}55$ Å^{-1}, the limit achievable on the D10 diffractometer. Averaging of symmetry-related reflexions led to 451 unique data. The internal consistency factor between symmetry related reflexions [comparable to $R(F^2)$] was 0·019.

Least-squares refinement with the program *LINEX* of the Buffalo computing system used starting parameters from the X-ray study and minimized $\sum w|F_o^2 - k^2F_c^2|^2$, where $w = 1/[\sigma^2(\text{counting}) + (0{\cdot}02F_o^2)^2]$. Extinction was treated isotropically in the type I Lorentzian approximation (Becker & Coppens, 1974, 1975). Extinction factors for all but three reflexions were 0·89 or higher. For the three strong b axis reflexions 020, 040 and 060, values of 0·61, 0·74 and 0·81 were obtained. Final R values are listed in Table 2.*

Table 2. *Refinement information*

g (isotropic extinction coefficient)	$0{\cdot}23\ (2) \times 10^{-4}$
Number of variables	83
$R = (\sum\|F_o - F_c\|^2/\sum F_o^2)^{1/2}$	0·026
$R_w = (\sum w\|F_o - F_c\|^2/\sum wF_o^2)^{1/2}$	0·029
$R(F^2) = (\sum\|F_o^2 - F_c^2\|/\sum F_o^2)^{1/2}$	0·026
$R_w(F^2) = (\sum w\|F_o^2 - F_c^2\|/\sum wF_o^2)^{1/2}$	0·050

Scattering lengths (10^{-12} cm): $b_O = 0{\cdot}58$, $b_N = 0{\cdot}938$, $b_C = 0{\cdot}665$, $b_H = -0{\cdot}374$.

Atomic parameters are compared with those of the refinement of the full set of X-ray data and the high order set (data above $\sin\theta/\lambda = 0{\cdot}75$ Å^{-1}) in Table 3. Due to the limited size of the data set, standard deviations are somewhat higher in the present study. However, the relatively long wavelength of the guide tube and the geometry of the D10 diffractometer do not allow data collection at higher $\sin\theta/\lambda$ values. It is clear that a higher limit must be achieved in further neutron diffraction studies at very low temperature.

* A list of structure factors has been deposited with the British Library Lending Division as Supplementary Publication No. SUP 31571 (4 pp.). Copies may be obtained through The Executive Secretary, International Union of Crystallography, 13 White Friars, Chester CH1 1NZ, England.

Table 3. *Atomic fractional coordinates* ($\times 10^4$) *and thermal parameters* (Å$^2 \times 10^4$) *for* (*a*) *the full set of X-ray data at* 30K, (*b*) *data above* $\sin\theta/\lambda = 0{\cdot}75$ Å^{-1}, (*c*) *the neutron data*

The temperature factor is expressed as

$$\exp[-2\pi^2(U_{11}a^{*2}h^2 + U_{22}b^{*2}k^2 + U_{33}c^{*2}l^2 + 2U_{13}a^*c^*hl)]\,.$$

Atomic coordinates

		a	*b*	*c*
O(1)	*x*	1308 (1)	1310 (1)	1310 (2)
	z	8064 (1)	8061 (1)	8062 (2)
O(2)	*x*	3881 (1)	3881 (1)	3879 (2)
	z	1331 (1)	1334 (1)	1340 (2)
O(3)	*x*	5179 (1)	5177 (1)	5174 (2)
	z	3183 (1)	3181 (1)	3190 (2)
N(4)	*x*	1993 (1)	1992 (2)	1991 (1)
	z	6819 (1)	6820 (1)	6821 (1)
N(5)	*x*	4220 (1)	4223 (1)	4224 (1)
	z	2815 (1)	2811 (1)	2811 (1)
C(6)	*x*	3065 (1)	3064 (1)	3065 (1)
	z	7172 (1)	7172 (1)	7171 (2)
C(7)	*x*	3813 (1)	3814 (1)	3812 (2)
	z	5879 (1)	5881 (1)	5878 (2)
C(8)	*x*	3448 (1)	3449 (1)	3447 (1)
	z	4206 (1)	4205 (1)	4202 (2)
C(9)	*x*	2364 (1)	2364 (1)	2362 (1)
	z	3831 (1)	3829 (1)	3827 (2)
C(10)	*x*	1644 (1)	1640 (1)	1644 (2)
	z	5162 (1)	5165 (1)	5162 (2)
H(C6)	*x*	3226 (13)		3255 (3)
	z	8364 (19)		8525 (5)
H(C7)	*x*	4600 (13)		4660 (3)
	z	6172 (19)		6183 (5)
H(C8)	*x*	2117 (12)		2068 (3)
	z	2657 (19)		2522 (4)
H(C10)	*x*	894 (12)		777 (3)
	z	4999 (18)		5002 (4)

Thermal parameters

		a	*b*	*c*
O(1)	U_{11}	70 (4)	65 (5)	47 (10)
	U_{22}	114 (3)	111 (3)	108 (9)
	U_{33}	82 (3)	82 (2)	93 (10)
	U_{13}	48 (2)	35 (2)	14 (8)
O(2)	U_{11}	107 (4)	97 (5)	88 (10)
	U_{22}	112 (3)	120 (3)	118 (9)
	U_{33}	52 (2)	57 (2)	55 (10)
	U_{13}	−10 (3)	−4 (2)	7 (9)
O(3)	U_{11}	39 (3)	51 (5)	28 (11)
	U_{22}	151 (3)	152 (3)	142 (10)
	U_{33}	109 (3)	96 (3)	97 (11)
	U_{13}	0 (3)	9 (2)	14 (8)
N(4)	U_{11}	55 (4)	43 (4)	42 (7)
	U_{22}	64 (3)	72 (3)	76 (6)
	U_{33}	63 (3)	65 (2)	72 (7)
	U_{13}	14 (3)	13 (2)	9 (5)
N(5)	U_{11}	61 (4)	55 (5)	57 (7)
	U_{22}	70 (3)	75 (3)	76 (6)
	U_{33}	68 (3)	61 (2)	69 (7)
	U_{13}	8 (3)	7 (2)	12 (5)

Table 3 (*cont.*)

C(6)	U_{11}	54 (4)	62 (5)	44 (9)
	U_{22}	82 (3)	85 (3)	85 (8)
	U_{33}	58 (3)	59 (3)	54 (11)
	U_{13}	−11 (3)	−2 (2)	−2 (7)
C(7)	U_{11}	52 (4)	52 (5)	44 (12)
	U_{22}	79 (3)	88 (3)	76 (8)
	U_{33}	62 (3)	58 (3)	68 (10)
	U_{13}	−9 (3)	−5 (2)	−16 (8)
C(8)	U_{11}	52 (4)	56 (5)	32 (9)
	U_{22}	71 (3)	74 (3)	76 (8)
	U_{33}	58 (3)	56 (3)	80 (9)
	U_{13}	15 (3)	6 (2)	14 (8)
C(9)	U_{11}	56 (4)	47 (5)	58 (9)
	U_{22}	75 (4)	80 (3)	66 (8)
	U_{33}	62 (3)	67 (3)	58 (11)
	U_{13}	−5 (3)	−2 (2)	−32 (8)
C(10)	U_{11}	50 (4)	56 (5)	37 (12)
	U_{22}	85 (4)	86 (3)	83 (9)
	U_{33}	73 (3)	70 (3)	66 (9)
	U_{13}	−8 (3)	2 (2)	8 (8)
H(C6)	U_{11}			154 (19)
	U_{22}			320 (20)
	U_{33}			142 (22)
	U_{13}			−29 (17)
H(C7)	U_{11}			76 (24)
	U_{22}			315 (20)
	U_{33}			201 (19)
	U_{13}			18 (15)
H(C9)	U_{11}			193 (19)
	U_{22}			308 (20)
	U_{33}			89 (21)
	U_{13}			−60 (18)
H(C10)	U_{11}			89 (26)
	U_{22}			326 (20)
	U_{33}			209 (21)
	U_{13}			−23 (16)

Atomic parameters

Bond lengths listed in Table 4 and given in Fig. 1 are in good agreement with those from the earlier X-ray study. The only systematic discrepancies are for the NO bonds which are about 0·007 Å shorter for the X-ray refinement. This effect, attributed to atomic asphericity (Coppens, 1974), is much smaller for the X-ray high-order refinement, the average remaining discrepancy being 0·002 Å.

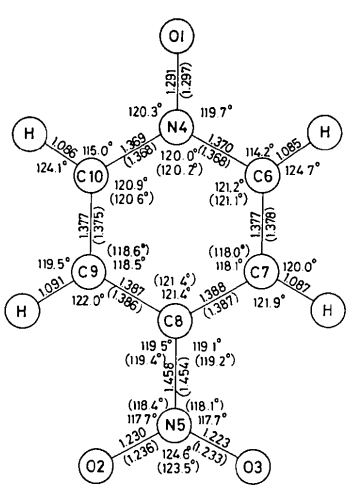

Fig. 1. Atom numbering, bond lengths and angles with the X-ray results in parentheses.

Table 4. *Bond lengths* (Å) (*not corrected for thermal motion*)

	X-ray	X-ray high order (NO only)	Neutron
O(1)—N(4)	1·297 (1)	1·292 (1)	1·291 (2)
O(2)—N(5)	1·236 (1)	1·227 (1)	1·230 (2)
O(3)—N(5)	1·233 (1)	1·227 (1)	1·223 (2)
N(4)—C(6)	1·368 (2)		1·370 (2)
N(4)—C(10)	1·368 (1)		1·369 (2)
N(5)—C(8)	1·454 (1)		1·458 (2)
C(6)—C(7)	1·378 (1)		1·377 (3)
C(7)—C(8)	1·387 (1)		1·388 (2)
C(8)—C(9)	1·386 (2)		1·387 (3)
C(9)—C(10)	1·375 (2)		1·377 (3)
C(6)—H(C6)	0·95 (1)		1·085 (4)
C(7)—H(C7)	1·01 (2)		1·087 (4)
C(9)—H(C9)	0·97 (1)		1·086 (4)
C(10)–H(C10)	0·95 (1)		1·091 (5)

The temperature parameters at 30K are quite small, especially for this 'soft' organic material. B values range from 0·2–1·2 Å^2, a typical value being 0·5 Å^2. All discrepancies between individual X-ray and neutron values are within the experimental errors. When the neutron U_{ii}'s for each of the non-hydrogen atoms are divided by the corresponding high-order X-ray parameters, ratios are obtained which average over all atoms to give: 0·82 for $i=1$, 0·96 for $i=2$ and 1·07 for $i=3$. This would suggest that the X-ray values for U_{11} are systematically high (or the neutron values low). However, the spread within the groups, especially for $i=1$, is such that no conclusions can be drawn about any systematic bias in either of the two data sets.

Electron density maps

Deformation density as a function of data cut-off

The X–N deformation densities in the molecular plane (at $y=\frac{1}{4}$) are given in Fig. 2 for $S_{max}=(\sin\theta/\lambda)_{max}$ $=0{\cdot}65$ and 0·75 Å^{-1} while other sections are represented in Figs. 4, 5 and 6. Scattering factors used were the same as in the X-ray analysis, while the scale factor for the calculated density was obtained by one cycle of least-squares refinement on the full X-ray data set with fixed neutron positional and thermal parameters. Additional maps, not reproduced here, have been calculated with cut-off values of 0·85 and 1·0 Å^{-1}. The average standard deviation is estimated as 0·07 e Å^{-3}. With increasing S_{max} the background noise increases considerably, but at the same time both bond and lone pair increase in height. An optimal data cut-off would balance the additional information to be gained against the increase in background level, but use of such a cut-off necessitates a correction for series termination in any quantitative application.

The effective scattering factor corresponding to a peak in the deformation density may be expressed as

$$f'(S)=f(S)\,.\,R(S)\,, \qquad (1)$$

where R is a resolution function which is 1 for $S<S_{max}$ and zero beyond. Thus, if $\mathcal{F}$ represents the Fourier transform operator and $*$ indicates a convolution between two functions, the electron density ϱ' is described by

$$\varrho'=\mathcal{F}[f']=\mathcal{F}[f\,.\,R]=\varrho * \mathcal{F}[R]\,, \qquad (2)$$

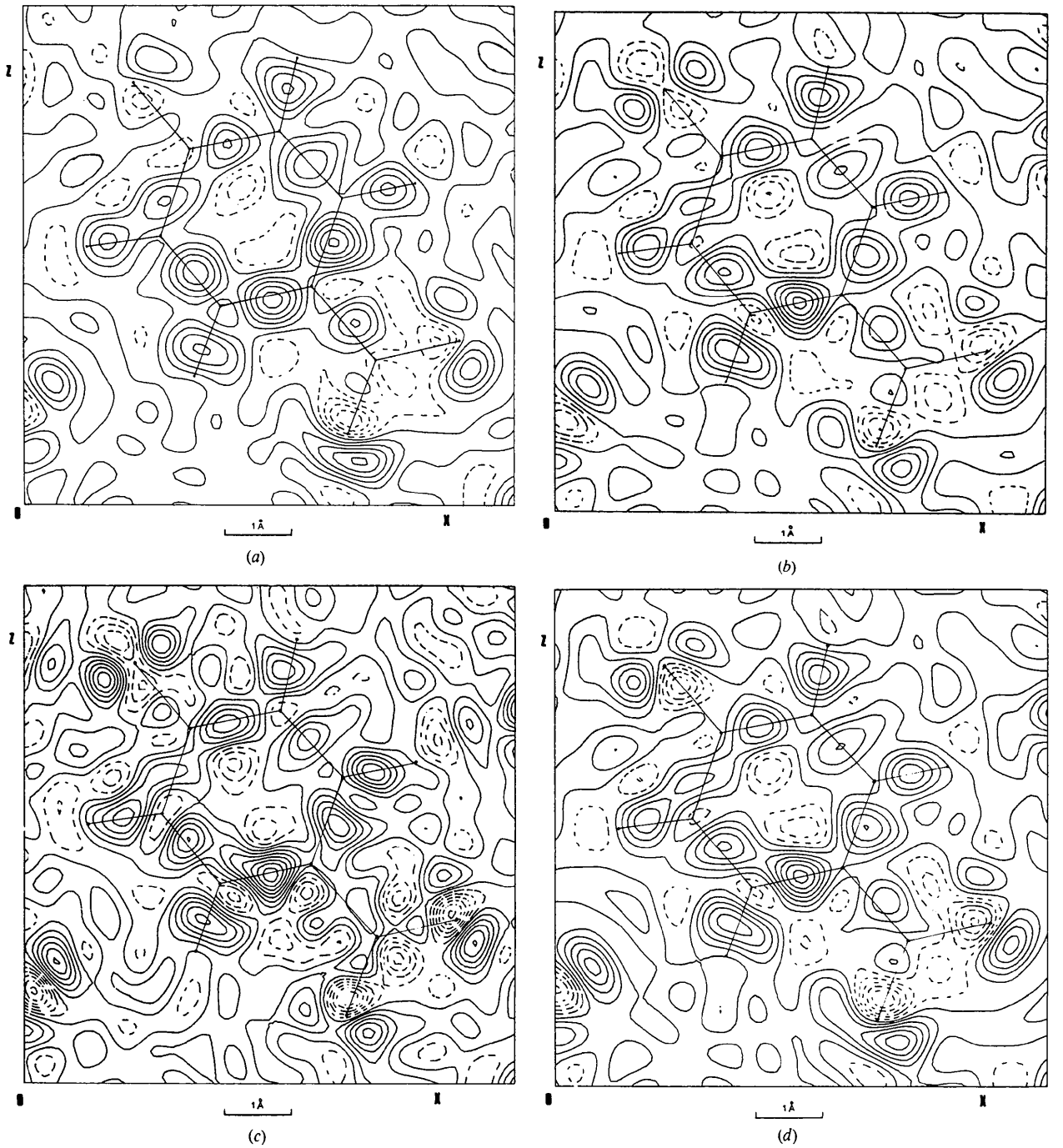

Fig. 2. Deformation maps where neutral spherical atoms are subtracted from the observed density based on the X-ray measurements by Wang, Blessing, Ross & Coppens (1976). The contours are at intervals of 0·1 e Å^{-3} and negative contours are dotted. All sections are coincident with the mirror plane at $y=\frac{1}{4}$. The following densities are given: (*a*) X–X_H, where X_H is calculated with atomic parameters from the high-order refinement of the X-ray data. $S_{max}=0{\cdot}65$ Å^{-1}; (*b*) X–N, where the neutron parameters are used for the calculated density N. $S_{max}=0{\cdot}65$ Å^{-1}; (*c*) same as (*b*), but $S_{max}=0{\cdot}75$ Å^{-1}; (*d*) X–N with all three oxygen positions used in the calculation moved 0·006 Å towards N. $S_{max}=0{\cdot}65$ Å^{-1}.

where ϱ is the distribution in the peak at infinite resolution.

Equation (2) indicates, as might be expected, that the effect of series termination is less severe the more diffuse the rest density in the peak under consideration. To analyse the series termination effect we have analysed peak heights as a function of S_{max}. Since peaks in bonds are generally more diffuse than lone-pair peaks (Coppens, 1974) all CC and CN and the O lone-pair peak heights were averaged separately. The points reproduced in Fig. 3 indicate that at the low temperature of the experiment both bond and lone-pair peaks have not yet reached their true height at $S_{max}=1$ Å^{-1}, which is the limit of the available X-ray data. The crossing of the two curves is a result of the relative diffuseness of the bond peaks and reminiscent of the effect of thermal smearing on the theoretical peak heights in dicyanogen analysed in a single Gaussian approximation (Coppens, 1974). As will be described in more detail elsewhere (Lehmann & Coppens, 1976) we have evaluated equation (2) analytically, again using a single Gaussian approximation for the bond peaks and adjusting the Gaussian exponent and the peak height at infinite resolution $\varrho(0)$ to give a best least-squares fit to the observed points. From the expression

$$\varrho(r)=\varrho(0)\exp(-\alpha r^2),$$

the fit shown in Fig. 3 is obtained with α_{bond} and $\alpha_{lone\ pair}$=10·3 and 17·3 Å^{-2} respectively, and infinite resolution peak heights of 0·61 e Å^{-3} for the average bond and 0·81 e Å^{-3} for the lone-pair peak.

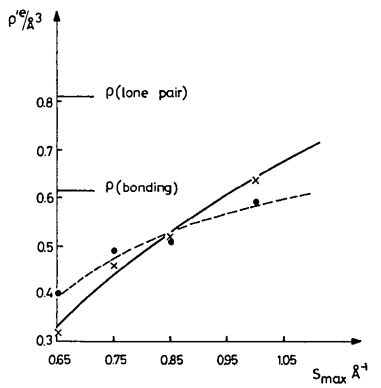

Fig. 3. The maximum value of the X–N deformation density in the bonding region and lone pairs, $\varrho'(0)$, as a function of the cut-off value S_{max} in the Fourier summation. Circles are average values for the maximum in CC and CN bonds, crosses are average of maximum value in the lone-pair region. The limits for infinite resolution, $\varrho(0)$, are indicated as well as the line describing the best least-squares fit.

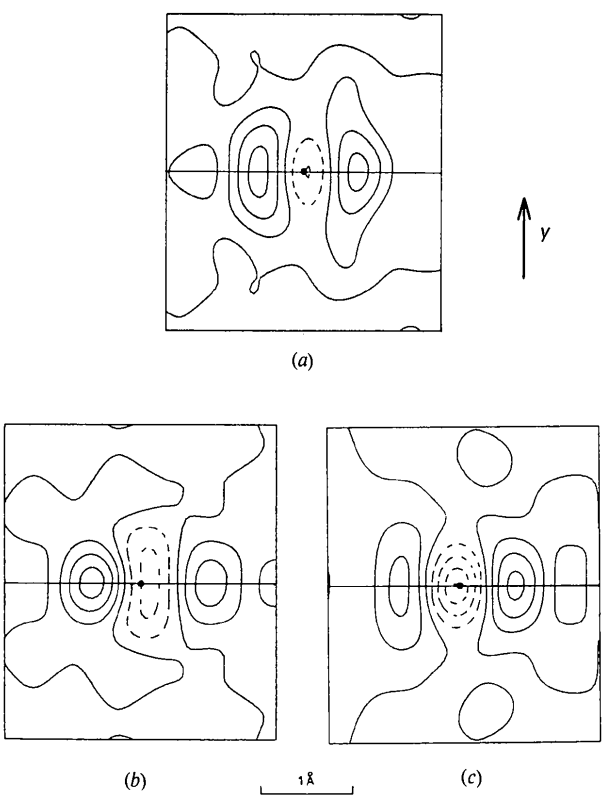

Fig. 4. Section of X–N density through the O atom orthogonal to the NO bonds. Contours and calculation identical to Fig. 2(*b*). The *y* axis is vertical and the mirror plane and O atom position are indicated. The view direction is along the NO bond direction. (*a*) Section through O(1), (*b*) section through O(2), (*c*) section through O(3).

Fig. 3 clearly indicates the necessity of correction for series termination in very low temperature studies if no accurate very high order data are available. The lone-pair curve suggests that such data should extend at least to the Mo limit. The weakness of the reflexions at high Bragg angles may dictate the use of a second, larger, specimen crystal to avoid unacceptable measuring times or excessive noise in the experimental densities.

Angular analysis of the lone-pair densities

A most striking difference in comparison with earlier work is the position of the lone-pair peaks at the O atoms. In studies of, for example, cyanuric acid (Coppens & Vos, 1971), α-glycine (Almlöf, Kvick & Thomas, 1973) and glycylglycine (Griffin & Coppens, 1975) O lone-pair peaks are observed at slightly less than 120° from the bond axis, while in other cases, notably cyano groups (Becker, Coppens & Ross, 1973; Matthews & Stucky, 1971) and the C≡O ligand (Rees & Coppens, 1973) lone-pair peaks are at 180° (Table 5). In *p*-nitropyridine *N*-oxide, which to our knowledge is the first compound studied containing either the nitro or nitroxo group, lone pairs are at about 90° at the nitroxo and at about 100° at the nitro group O atoms (see also perpendicular cross sections in Fig. 4).

In order to ascertain that the position of these lone-pair peaks is not an artifact sensitive to small shifts in atomic positions, all three O positions used in calculating the spherical atom density were shifted by about three standard deviations in the neutron data

Table 5. *Position of lone-pair density at terminal atom as defined by the angle α between the bond and the vector connecting the terminal atom with the lone-pair peak*

–CO in organic molecules				–CO in metallo-organic ligands		
Cyanuric acid[a]	O(1)	121°		Benzene Cr tricarbonyl[e]		180°
	O(2)	*		Cr hexacarbonyl[f]		180
Glycylglycine[b]	O(2)	102	111	–CN		
		120		Tetracyanoethylene[g]		180
Oxalic acid[c]		140	115	–NO		
		89		*p*-Nitropyridine *N*-oxide[h]		
				Nitroxide	O(1) 79	89
					99	
α-Glycine[d]	O(1)	106	114			
		122		Nitro group	O(2) 111	
	O(2)	*			95	
					O(3) 85	101
					112	

* Broad single maximum. (*a*) Coppens & Vos, 1971, (*b*) Griffin & Coppens, 1975, (*c*) Coppens, Sabine, Delaplane & Ibers, 1969, (*d*) Almlöf, Kvick & Thomas, 1973, (*e*) Rees & Coppens, 1973, (*f*) Rees, 1976, (*g*) Becker, Coppens & Ross, 1973, (*h*) this study.

(0·006 Å) towards the adjacent N atom. The shifted map (at $S_{max}=0{\cdot}65$ Å^{-1}) [Fig. 2(*d*)] shows no evidence of drastic changes in lone-pair positions which remain at approximately 90° from the nitroxide bond axis. Furthermore, it should be noted here that the same feature also appears in a deformation density map based on the refinement of the coefficients describing deviation from spherical atom symmetry (Hirshfeld, 1975) using the same X-ray data (Wang, Blessing, Ross & Coppens, 1976). Thus the significance of the appearance of the lone-pair peak density in this region seems well established.

One distinction of the *p*-nitropyridine *N*-oxide crystals is that unlike the carbonyl compounds they contain no hydrogen bonds. However, no clear evidence exists for perturbation of the lone-pair density by hydrogen bonding, and theoretical studies (Dreyfus, Maigret & Pullman, 1970; Kollman & Allen, 1970) indicate such a large perturbation to be unlikely. We should note here that a very strongly hydrogen-bonded pyridine *N*-oxide molecule is found in its complex with trichloroacetic acid (Golič, Hadzi & Lazarini, 1971). A study of this complex is now being planned.

The difference between the lone-pair positions may be interpreted in terms of the hybridization of the terminal atoms. Though such hybridizations can only approximately account for the molecular charge density they provide a convenient framework for interpretation that is justified by analysis of localized molecular orbitals from self-consistent field calculations (Newton & Schulman, 1972). A hybridization scheme corresponding to the observed lone-pair positions is given in Table 6. It indicates decreasing *s* character in the σ bonding orbital in the direction carbonyl → nitroxo, *i.e.* when the atom to which O is bound becomes more electronegative. This is in agreement with concepts developed by Bent (1961) who has argued that more *p* character will be found in bonding hybrids to more electronegative atoms. To achieve the hybridization of the CO oxygen specified in Table 6, $\frac{1}{3}$ of an *s* electron has been promoted to a 2*p* orbital, which would require about 65 kcal mol^{-1} (Coulson, 1961). This energy must be retrieved by the more efficient bonding of the σ sp^2 bonding hybrid, which is more readily accomplished with the more diffuse C atom bonding hybrids than with N.

Table 6. *Terminal atom hybridization corresponding to the observed lone-pair positions* (*z axis along bond*)

	σ bonding	π bonding	Lone pair(s)	Number of *s* electrons
CO (carbonyl in organic molecules)	sp^2	p_y	$(sp^2)^2,(sp^2)^2$	$\frac{5}{3}$
CO (ligand) CN (cyano group)	sp	p_x,p_y	$(sp)^2$	$\frac{3}{2}$
NO (nitroxide group)	p_z	p_y	s^2,p_x^2	2

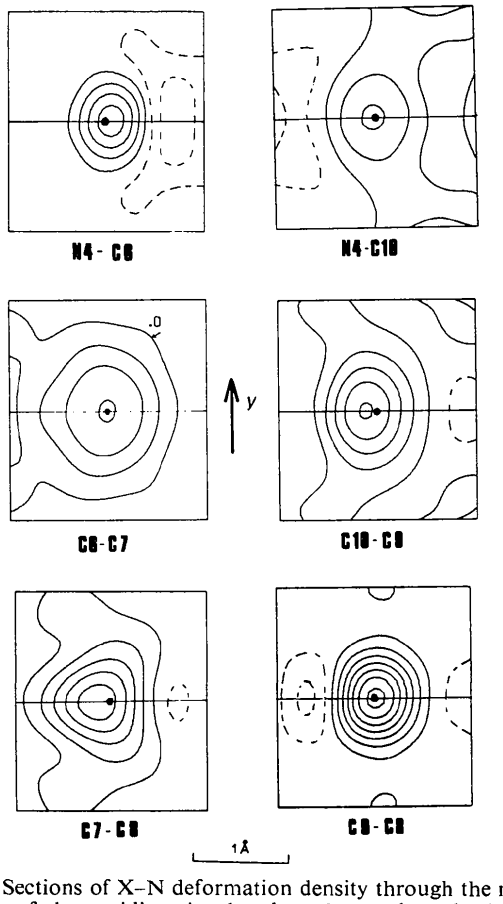

Fig. 5. Sections of X–N deformation density through the midpoint of the pyridine ring bonds orthogonal to the bond. Contours as in Fig. 2. $S_{max}=0{\cdot}65$ Å^{-1}. The mirror plane and the bond intersection with the sections are indicated. For the left column of sections the pyridine ring centre is to the right and for the right column the centre is to the left.

The trend observed here is further supported by the deformation density in Cl_2 (Stevens & Coppens, 1976), which similarly indicates lone-pair density at 90° from the bond axis.

The bond peaks

Bond peaks in the plane of the molecule show left–right symmetry within the estimated standard deviations. The peaks are extended perpendicular to the molecular plane, indicating partial π character (Fig. 5). Fig. 6 shows sections 0·3 and 0·6 Å above the molecular plane.

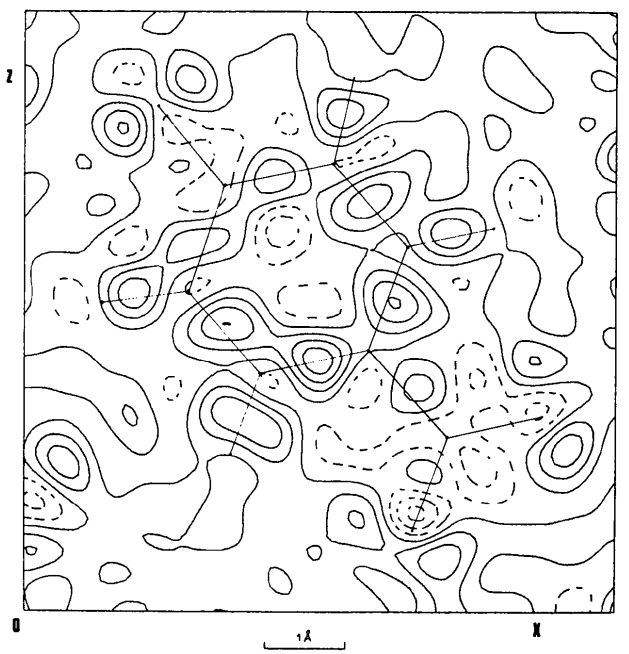

(*a*)

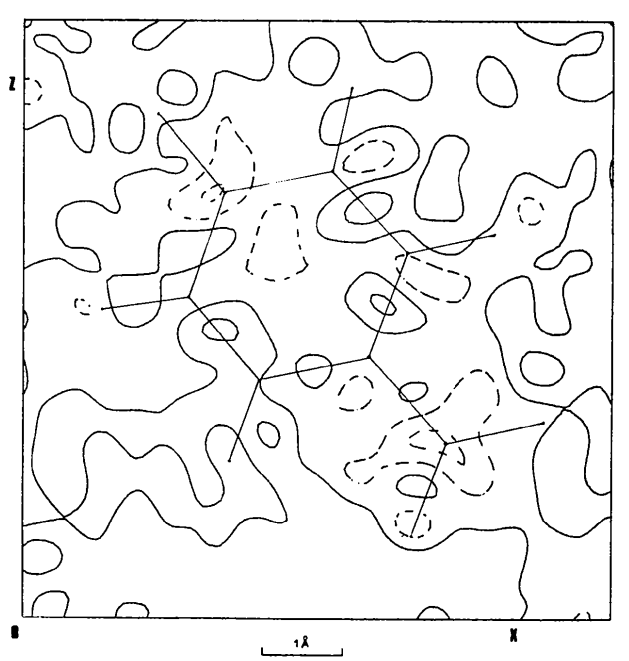

(*b*)

Fig. 6. X–N deformation density (*a*) 0·3 and (*b*) 0·6 Å above the molecular plane. Contours as in Fig. 2. $S_{max}=0{\cdot}65$ Å^{-1}.

None of the NO bonds shows deformation density at or near its midpoint. This does not imply absence of covalency, because subtraction of a 'prepared' non-spherical atom, with only one electron in the σ bonding orbital, would enhance the difference density in the bond region. We have not used this alternative difference map, taking the position with Rosenfeld (1964) and with Ransil & Sinai (1967) that the preparation of the non-spherical atom is an intermediate step in bonding so that the alternative maps do not correspond to charge migration upon molecule formation.

The absence of deformation density in the NO bonds raises the question of the balance of electrostatic forces on the O atom, required by the Hellmann–Feynman principle. As discussed by Hirshfeld & Rzotkiewicz (1974) in the promolecule, defined as the superposition of spherical atoms, electrostatic balance is absent because of the penetration of one atom into the charge cloud of its neighbour. In the real molecule this penetration field must be balanced to achieve equilibrium by the migration field, the electrostatic force exerted by the deformation density. The complete absence of experimental density in the NO bonds, which are electrostatic binding regions (Berlin, 1951), is therefore difficult to understand. Some bond density could be present within the experimental standard deviations, but this does not satisfactorily answer the consistent appearance of this effect in all three NO bonds in *p*-nitropyridine *N*-oxide, in uronium nitrate (de With, Harkema & Feil, 1975) and in the Cl_2 molecule (Stevens & Coppens, 1976). One possible explanation is the existence of a polarization of electrons near the nuclei, which would be important for electrostatic balance, but not detectable within the resolution of the X-ray experiment.

Conclusions

The increase of peak height with data cut-off indicates that quantitative measurement of electron densities at low temperatures requires either a correction for series termination or the collection of very high order data on a relatively large crystal. The latter procedure is obviously preferable and may be essential in quantitative testing of advanced theoretical calculations.

The difference in hybridization of terminal atoms in different groups as derived from the position of the lone-pair peaks typifies the qualitative information of chemical importance that can be obtained from charge density studies.

The lack of experimental deformation density in some of the bonds requires further analysis.

We are indebted to Dr W. B. Yelon for help and guidance in using the diffractometer D10 and to Dr

P. J. Brown for use of her Fourier plotting programs. Encouragement of this work by Professor E. F. Bertaut is gratefully acknowledged.

References

ALMLÖF, J., KVICK, A. & THOMAS, J. O. (1973). *J. Chem. Phys.* **59**, 3901–3910.

BECKER, P. J. & COPPENS, P. (1974). *Acta Cryst.* A**30**, 129–147.

BECKER, P. J. & COPPENS, P. (1975). *Acta Cryst.* A**31**, 417–425.

BECKER, P. J., COPPENS, P. & ROSS, F. K. (1973). *J. Amer. Chem. Soc.* **95**, 7604–7609.

BENT, H. A. (1961). *Chem. Rev.* **61**, 275–311.

BERLIN, T. (1951). *J. Chem. Phys.* **19**, 208–213.

CLAUDET, G. M., TIPPE, A. & YELON, W. B. (1976). *J. Phys. E.* To be published.

COPPENS, P. (1974). *Acta Cryst.* B**30**, 255–261.

COPPENS, P., SABINE, T. M., DELAPLANE, R. G. & IBERS, J. A. (1969). *Acta Cryst.* B**25**, 2451–2458.

COPPENS, P. & VOS, A. (1971). *Acta Cryst.* B**27**, 146–158.

COULSON, C. A. (1961). *Valence*. Oxford Univ. Press.

DREYFUS, M., MAIGRET, B. & PULLMAN, A. (1970). *Theoret. Chim. Acta*, **17**, 109–119.

GOLIČ, L., HADZI, D. & LAZARINI, F. (1971). *Chem. Commun.* p. 860.

GRIFFIN, J. F. & COPPENS, P. (1975). *J. Amer. Chem. Soc.* **97**, 3496–3505.

HIRSHFELD, F. L. (1975). Private communication.

HIRSHFELD, F. L. & RZOTKIEWICZ, S. (1974). *Mol. Phys.* **27**, 1319–1343.

KOLLMAN, P. A. & ALLEN, L. C. (1970). *J. Chem. Phys.* **52**, 5085–5094.

LEHMANN, M. S. & COPPENS, P. (1976). To be published.

LEHMANN, M. S. & LARSEN, F. K. (1974). *Acta Cryst.* A**30**, 580–584.

MATTHEWS, D. A. & STUCKY, G. D. (1971). *J. Amer. Chem. Soc.* **93**, 5954–5963.

NEWTON, M. D. & SCHULMAN, J. M. (1972). *J. Amer. Chem. Soc.* **94**, 767–773, 773–778.

RANSIL, B. J. & SINAI, J. J. (1967). *J. Chem. Phys.* **46**, 4050–4074.

REES, B. (1976). *Acta Cryst.* A**32**, 483–488.

REES, B. & COPPENS, P. (1973). *Acta Cryst.* B**29**, 2515–2524.

ROSENFELD, J. L. J. (1964). *Acta Chem. Scand.* **18**, 1719–1730.

STEVENS, E. D. & COPPENS, P. (1976). To be published.

WANG, Y., BLESSING, R. H., ROSS, F. K. & COPPENS, P. (1976). *Acta Cryst.* B**32**, 572–578.

WITH, G. DE, HARKEMA, S. & FEIL, D. (1975). *Acta Cryst.* A**31**, S227–S228.

Acta Cryst. (1976). B**32**, 1784

The Crystal Structure of Calcium Borate Chloride $CaCl_2 . Ca_3(BO_3)_2$

BY Z. ŽAK

Department of Inorganic Chemistry, J. E. Purkyně University, Kotlářská 2, 611 37 *Brno, Czechoslovakia*

AND F. HANIC

Institute of Inorganic Chemistry, Slovak Academy of Sciences, Dúbravská cesta, 809 34 *Bratislava, Czechoslovakia*

(*Received* 22 *September* 1975; *accepted* 12 *December* 1975)

The structure of $CaCl_2 . Ca_3(BO_3)_2$ has been determined by direct methods. The effect of rationally dependent atomic coordinates on the phase-determining procedure is described. The structure consists of Ca^{2+}, Cl^- and BO_3^{3-} ions arranged in distinct, mutually alternating anionic and cationic layers parallel to (102). The BO_3 groups are practically planar with B–O = 1·403, 1·391 and 1·390 Å. The sevenfold coordination around Ca is represented by two types of polyhedra, $CaCl_3O_4$ and $CaCl_2O_5$. Each O atom is surrounded by three Ca atoms and one B atom in the form of a slightly distorted tetrahedron. The e.s.d.'s for the bond lengths are 0·001–0·003 Å, for the bond angles 0·02–0·25°. The final R is 0·037.

Introduction

Ca_2BO_3Cl is an intermediate phase in the system $Ca_3(BO_3)_2$–$CaCl_2$ (Majling, Figusch, Čorba & Hanic, 1974). The existence of two different coordination numbers, triangular or tetrahedral, in borate structures and the fact that the O atoms in oxy-ions may be replaced by halogen atoms to form oxy-halide ions, $MO_aX_b^{n-}$, raised a question as to whether Ca_2BO_3Cl is calcium borate chloride $CaCl_2 . Ca_3(BO_3)_2$, or calcium chloroborate, $Ca_2(BO_3Cl)$.

Crystallographic and intensity data

Recently, the crystal data for Ca_2BO_3Cl were published (Majling *et al.*, 1974): $a = 3·9484$ (4), $b = 8·692$ (2), $c = 12·402$ (2) Å, $\beta = 100·27$ (1)°, $V = 418·8$ Å^3, $Z = 4$, $D_m = 2·76$ (1), $D_x = 2·77$ g cm^{-3}, space group $P2_1/c$.

Single crystals prepared according to Majling *et al.* (1974) were twinned, (010) being the plane of twinning as determined from Weissenberg photographs. The crystal used for the structure determination had to be cut from a twin in the form of a triangular prism with